

Wide-Field Surface-Enhanced Coherent Anti-Stokes Raman Scattering Microscopy

Cheng Zong, Ran Cheng, Fukai Chen, Peng Lin, Meng Zhang, Zhicong Chen, Chuan Li, Chen Yang, and Ji-Xin Cheng*



Cite This: <https://doi.org/10.1021/acsp Photonics.1c02015>



Read Online

ACCESS |



Metrics & More



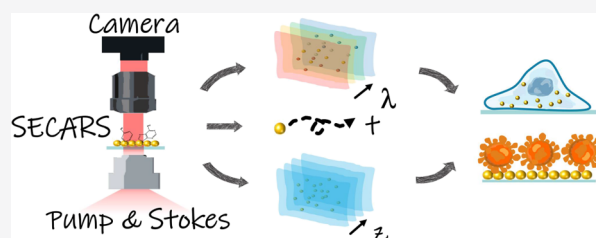
Article Recommendations



Supporting Information

ABSTRACT: Surface-enhanced Raman scattering (SERS) spectroscopy has been used extensively to study biology, chemistry, and materials. However, point-by-point SERS mapping is time-consuming, taking minutes to hours for large-scale imaging. Here, we report a wide-field surface-enhanced coherent anti-Stokes Raman scattering (WISE-CARS) microscope for monitoring nanotags in live cells and label-free detection of metabolic molecules. The WISE-CARS microscope achieves an imaging speed of 120 fps for a field of view of $130 \mu\text{m} \times 130 \mu\text{m}$. By spectral focusing of femtosecond lasers, a hyperspectral WISE-CARS stack of 60 frames can be acquired within 0.5 s, where over 1 million Raman spectra are parallelly recorded with a spectral resolution of 10 cm^{-1} . As applications, we demonstrate time-lapse, three-dimensional (3D) WISE-CARS imaging of nanotags in live cells as well as label-free detection of adenine released from *S. aureus*.

KEYWORDS: wide-field microscopy, surface-enhanced coherent anti-Stokes Raman scattering, hyperspectral imaging, 3D live-cell imaging, label-free biomolecular imaging



INTRODUCTION

Surface-enhanced Raman spectroscopy (SERS) is a powerful vibrational spectroscopy technique that allows for highly sensitive detection of low concentration analytes, even down to a single-molecule level.^{1,2} Because of the localized surface plasmon resonance (LSPR), an extremely large local electromagnetic field is generated on the metal surface to amplify the Raman signals of molecules closely associated with the nanostructure.^{3,4} However, most of the instrumentations used for SERS imaging rely on mechanical scanning.⁵ For large-area imaging, the time-consuming point-by-point scanning process with an acquisition time of a few seconds at each pixel often takes minutes to hours for mapping the SERS spectra of a sample.⁶

With high-speed cameras and tunable filters, wide-field SERS imaging has been developed to meet the need for large-scale Raman imaging.^{7–10} Among these technologies, wide-field hyperspectral imaging is achieved by utilizing tunable bandpass filters, such as liquid crystal tunable filters^{9,10} or angle-dependent filters,^{7,8} to scan a Raman spectral window. However, the spectral resolution of tunable filters is limited to tens of wavenumbers. In addition, the wavelength tuning speed per step is about hundreds of milliseconds, which limits the hyperspectral imaging speed.

Coherent anti-Stokes Raman scattering (CARS) has demonstrated great potential for biomedical imaging.^{11–14} Compared to sample-scan spontaneous Raman microscopy, CARS imaging is typically carried out by scanning the lasers

and collecting the signals with a point detector (a photomultiplier tube or an avalanche photodiode). CARS microscopy enables high-speed chemical imaging of living systems up to the video rate.¹⁵ To achieve higher sensitivities, surface plasmon resonance has been employed to enhance CARS signals^{16–19} and the single-molecule detection via surface-enhanced CARS (SECARS) has been verified.^{20–22} Thus far, SECARS imaging has been implemented in the scanning mode, where the imaging speed for hyperspectral data acquisition is limited.

To achieve faster CARS imaging, alternative excitation geometries based on wide-field illumination have been developed. Early wide-field CARS setup used a dark-field condenser to focus pump light and to counter-propagate the Stokes beam to satisfy the phase-matching condition.²³ Later, simpler illumination geometries such as defocused laser beams²⁴ and oblique-incidence illumination schemes^{25–27} were adopted. Such nonphase-matched illuminations rely on the strongly scattering samples to redirect the light path. The video-rate wide-field CARS imaging and even single-shot imaging of biological samples have been demonstrated.^{24,27}

Received: December 29, 2021

However, all these schemes are based on single-color CARS.²⁸ High-speed hyperspectral CARS imaging with wide-field illumination and high detection sensitivity remains to be explored. Recently, Potma et al. employed wide-field evanescent illumination in CARS microscopy, where surface plasmon polariton (SPP) from 30 nm gold film enhanced the CARS signals of organic films and dried cells.^{29,30} However, the coherent SPP induces flares and an interfering pattern in the image and cannot be used for imaging into a live cell.

Here, we demonstrate a wide-field surface-enhanced coherent anti-Stokes Raman scattering (WISE-CARS) microscope that enables ultrahigh-speed chemical imaging. Our method takes full advantage of SECARS. First, the power density in SECARS is 1000 times lower than that in conventional CARS microscopy without plasmonic enhancement.³¹ This low power requirement opens the opportunity for wide-field illumination and parallel data collection. Second, the main issue in wide-field CARS microscopy, the phase-matching condition over the whole field of view,²³ is relaxed in WISE-CARS. Because SECARS signals are excited by the local electric fields from nanostructures, the signals can be generated without controlling the directions of the excitation beams to match the far-field phase-matching condition. Third, we utilize a spectral focusing approach for fast-tuning the beating frequency between pump and Stokes beams, which allows ultrahigh-speed hyperspectral CARS imaging. Specifically, we demonstrate hyperspectral SECARS imaging of molecules on a substrate composed of self-assembled monolayered Au nanoparticles (NPs) at a speed of 120 frames per second (fps). This speed is faster than typical laser-scanning CARS (~1 fps) by two orders of magnitude. Then, we illustrate the system's capability by WISE-CARS imaging of live cells at 60 fps and three-dimensional (3D) imaging of nanotags in live cells within 1 s. Furthermore, we demonstrate label-free detection of adenine, an endogenous biomolecule released from starved *S. aureus*, via WISE-CARS microscopy.

EXPERIMENTAL SECTION

Hyperspectral Wide-Field CARS Microscope. The schematic is shown in Figure 1a. In brief, a femtosecond laser (Spectra-physics, InSight DS) with an 80 MHz repetition rate provides a tunable pump (680–1350 nm) beam and a fixed Stokes (1040 nm) beam. The pump and Stokes beams are combined on a dichroic beam splitter and then both are chirped by 5 × 15 cm glass rods (SF57, SCHOTT) for spectral focusing purposes. For equal stretching, the Stokes pulse is chirped by an additional 15 cm glass rod (SF57, SCHOTT) before combination. Under such a chirping condition, the spectral resolution of our setup reaches 10 cm⁻¹.³² Then, combined beams are expanded two times by a lens pair for increasing the field of view. The combined beams are focused with a 250 mm achromatic lens on the back focal plane of a 20×, 0.4 NA objective (Olympus) to provide wide-field illumination. The illuminated area at the sample is around 130 μm × 130 μm (Figure 1b). After the sample, the forward scattered beam is collected by a 60×, 1.2 NA water immersion objective (Olympus). The sample image is projected onto a CMOS camera (Grasshopper3, FLIR) through a tube lens with a focal length of 180 mm. The CMOS camera allows an imaging speed as high as 120 fps. Each frame contains 1224 × 1024 pixels, with a pixel size of 0.13 μm. Bandpass filters before the camera block the excitation light and passes the CARS

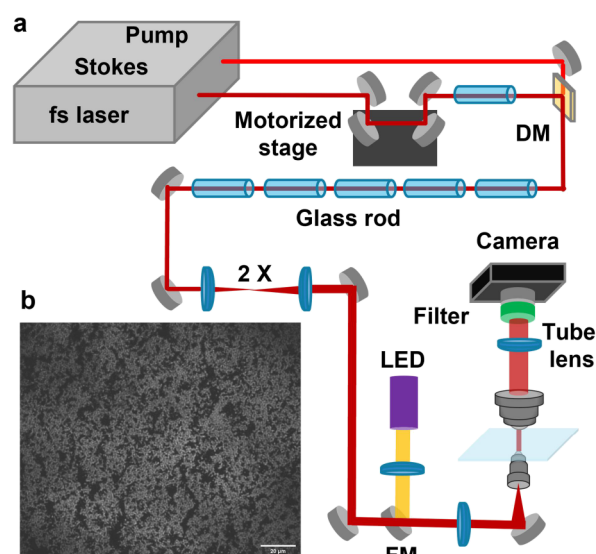


Figure 1. Hyperspectral wide-field SECARS microscope. (a) Schematic. DM: dichroic mirror; FM: flipper mirror. (b) Bright-field view of the aggregated Au NP substrate. Scale bar: 20 μm.

signal. A light-emitting diode (LED) is used for bright-field imaging.

To obtain hyperspectral information, a motorized linear stage is installed in the Stokes beam for tuning the delay between the chirped pump and Stokes beams. The motorized stage and the CMOS camera are synchronously triggered. When the camera is exposed, the motorized stage starts a uniform linear motion at a specific speed. For example, with a commonly used delay distance = 1.2 mm, the velocity of the stage is 1.2 mm per second, and the frame rate of the camera is 60 fps. In this condition, the hyperspectral CARS data cube with 60 Raman channels is obtained within 1 s.

To obtain 3D sections, a piezoelectric objective lens positioner (MIPOS100 Piezosystem Jena) is used to control the focus of the collection objective. The piezo positioner and the camera are also synchronized. The piezo positioner scans from the bottom to the top at a constant speed when the camera captures images.

Preparations of Au NPs for WISE-CARS Detection.

The Au nanoparticles (Au NPs) are prepared using the citrate reduction method,³³ resulting in particles with diameters of 40 to 50 nm. Three different samples are prepared for WISE-CARS imaging. The first sample is an aggregated Au NP substrate for large-area imaging. Au NPs colloidal suspension (0.5 mL) is concentrated to 2 to 4 μL by centrifuging, which is then added to 5 μL of analyte solution. The analyte solution induces the aggregation of Au NPs. The aggregated Au NPs are dropped on a cover glass, followed by vacuum drying to obtain the substrate for SECARS imaging of analytes.

Second, 4-mercaptopyridine (Mpy)-modified Au nanotags are prepared for live-cell imaging. To prepare the nanotags, the as-prepared 5 mL Au NPs are subsequently functionalized with Mpy by adding 50 μL of 54 μM Mpy aqueous solution drop-by-drop under vigorous shaking. To increase the stability of the Mpy-functionalized Au NPs colloid, 50 μL of 2% bovine serum albumin aqueous solution is added dropwise under vigorous stirring and is kept shaking for 15 min.³⁴

Third, as described in our previous study,³¹ self-assembled, monolayered substrates of AuNPs are prepared for label-free detection of biomolecules. In brief, homogeneous Au NPs with

a diameter of 110 nm are synthesized using a two-step seed-mediated growing method.³⁵ The cleaned cover glass is silanized in 10% (v/v) of (3-aminopropyl)-trimethoxysilane ethanol solution for 24 h and then baked at 110 °C for 2 h. Finally, the cover glass is immersed in the above 110 nm Au NP solution for 20 h to assemble the Au NPs.³⁵

Cell Culture for Live-Cell Imaging. T24 cells are cultured in Dulbecco's modified eagle medium (DMEM) with 10% fetal bovine serum and 1% penicillin–streptomycin. The suspended T24 cells are seeded on a glass-bottom dish and cultured 48 h for cell attachment. Nanotags (1 mL) are centrifuged, and the supernatant is removed. The concentrated nanotags are added into the culture medium to interact with cells for 8 h. After that, the culture medium is discarded, and the cells are washed three times by phosphate-buffered saline (PBS) to remove the free-moving nanoparticles. Finally, 2 mL of PBS is added into the culture dish again before WISE-CARS imaging.

S. aureus bacteria are cultured in Mueller Hinton broth and are harvested at the log phase. The bacteria are washed three times with 1 mL of water. The bacterial pellet is suspended in 20 μ L of water, and 2 μ L of the resulting bacterial suspension is dropped and dried onto the self-assembled Au NP substrate. Samples are dried onto the Au substrate either immediately (0 h) or after 1 h in order to study the cellular response to the starvation stress.

Data Processing. The camera, motorized stage, and piezoelectric positioner are controlled by MATLAB (Math-Works). The data are collected and processed by MATLAB. BM4D is used to denoise the SECARS data.³⁶ The AirPLS method is used for background removal.

RESULTS

Hyperspectral WISE-CARS Imaging of Molecules Adsorbed to Au NPs. To demonstrate hyperspectral WISE-CARS, we first show the results obtained from the aggregates of Mpy-modified Au NPs. The pump laser centered at 891 nm was employed to produce a SECARS spectrum covering a window ranging from 1520 to 1680 cm^{-1} . The pump and Stokes laser powers were both set to 150 mW. A hyperspectral data cube (1224 \times 1024 \times 60) was recorded at a speed of 60 fps. Figure 2a shows the SECARS image of Mpy-modified aggregates of Au NPs at 1577 cm^{-1} . The hyperspectral data cube is shown in Video S1. The pattern shows the heterogeneity of the aggregates of Au NPs. Figure 2b shows the representative single-pixel SECARS spectra of Mpy and SERS spectra of Mpy (bottom). The two peaks at 1577 and 1612 cm^{-1} can be observed in single-pixel SECARS spectra. The relative intensities of these two peaks relate to the adsorbing conditions of Mpy on Au NPs.³⁵

To further demonstrate the capability of high-speed hyperspectral imaging, we prepared an ATTO740-modified self-assembled Au NP substrate. To cover the desired spectral window, the pump beam was tuned to 888 nm. The powers of pump and Stokes lasers were both 120 mW. With 120 fps imaging speed, it only took us 0.5 s to obtain the hyperspectral data cube (1224 \times 1024 \times 60) of ATTO740 on Au NPs. In this condition, the velocity of the motorized stage was 2.4 mm per second. The SECARS image at 1640 cm^{-1} is shown in Figure 2c. Figure 2d presents the representative single-pixel SECARS spectra and the SERS spectrum (bottom) of ATTO740 on Au NPs. The single peak at 1640 cm^{-1} is clearly observed in SECARS spectra and in the SERS spectrum. Hence, we successfully demonstrate the ability of

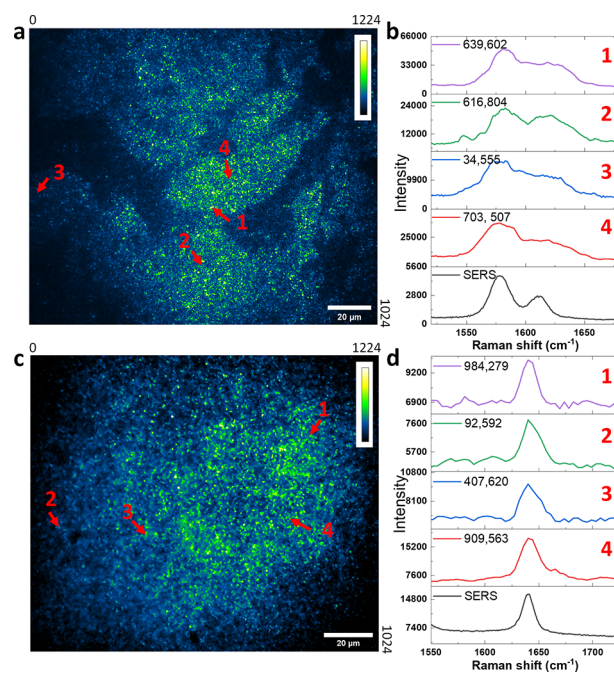


Figure 2. Hyperspectral WISE-CARS imaging of the Au NP substrate. (a) SECARS image of Mpy adsorbed on aggregated Au NPs. Speed: 60 fps. (b) Single-pixel SECARS spectra of Mpy from indicated locations and the SERS spectrum of Mpy (bottom). (c) SECARS image of ATTO740 adsorbed on the self-assembled Au NP substrate. Speed: 120 fps. (d) Single-pixel SECARS spectra of ATTO740 from the indicated locations and the SERS spectrum of ATTO740 (bottom). The scale bar is 20 μ m. The inside labels show the X–Y pixel coordinates where the spectra were recorded. Red arrows indicate the corresponding locations in the image.

WISE-CARS to parallelly record over 1 million SECARS spectra in 0.5 s.

Dynamic WISE-CARS Imaging of Nanotags in Live Cells. To demonstrate the capability of imaging dynamic live cells, we incubated T24 cells with Mpy-modified Au nanotags for 8 h (Figure 3a). The Au NPs were expected to enter cells by endocytosis and thereafter enclosed within endosomes or lysosomes.³⁷ To record the movements of nanotags, we choose the Raman signature band of Mpy at 1577 cm^{-1} . The frame rate was 16.6 ms per 1224 \times 1024 pixel image. With a frame acquisition time as short as 16.6 ms, a 60-frame video was recorded to show the movements of nanotags inside a live cell during a 1 s period (see Video S2). Figure 3b shows the SECARS image of live T24 cells at 1577 cm^{-1} . The bright spots indicate the locations of Au nanotags. As shown in Figure 3c, the time-lapse recording provides spatiotemporal dynamics of nanotags such as spatial movements and intensity blinking, suggesting rapid changes of nanoparticles in live cells on the level of milliseconds. In addition, the SECARS signals of some nanotags show significant intensity fluctuations while others rarely show intensity changes. This result suggests the versatile dynamics of nanoparticles inside a living cell.

To demonstrate hyperspectral SECARS imaging of nanotags in living cells, we simultaneously scanned the delay stage and recorded the image stack in 1 s at the speed of 60 fps. The hyperspectral SECARS imaging stack of live cells is shown in Video S3. Figure 3d presents the representative single-pixel SECARS spectra. The two peaks of Mpy located at 1577 and 1612 cm^{-1} are clearly observed. The ratio between the two

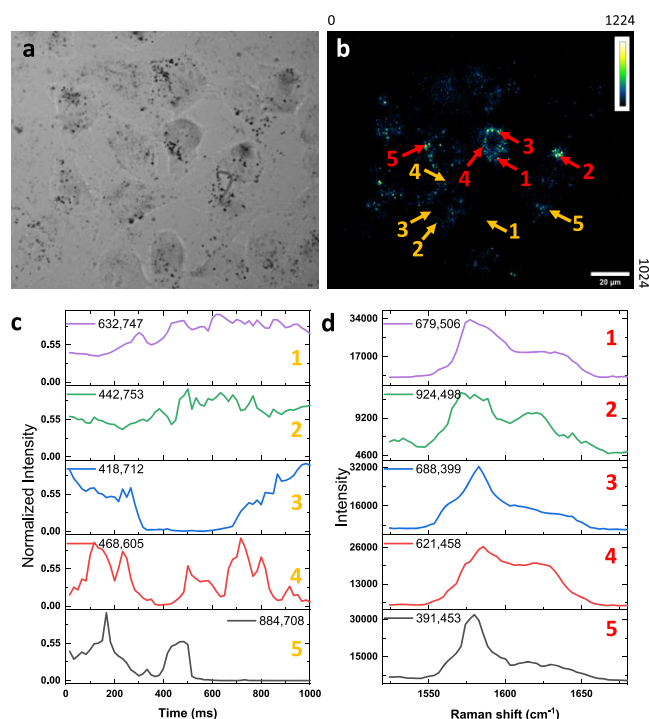


Figure 3. Hyperspectral WISE-CARS imaging of live cells. (a) Bright-field image of T24 cells illuminated by LED. (b) Corresponding SECARS image of T24 cells at 1577 cm⁻¹. (c) Time-lapse curves of single clusters. (d) Single-pixel SECARS spectra of nanotags in live cells. The scale bar is 20 μm. Inside labels show the X–Y pixel coordinates where the spectra were recorded. Yellow arrows indicate where time-lapse curves are selected in the image. Red arrows show the locations where single-pixel spectra are selected.

peaks is different because the Mpy is a pH-sensitive molecule. The different ratios indicate that the nanotags exist in different stages of the endocytic process, including early endosomes (pH 6.0–6.5), late endosomes (pH 5.5), and lysosomes (pH 4.0–5.0).³⁷ This result indicates that hyperspectral WISE-CARS could monitor the cellular environment in live cells.

3D WISE-CARS Imaging of Nanotags in Live Cells. To demonstrate the 3D imaging ability of WISE-CARS, we treated live T24 cells with Mpy-modified Au NP nanotags for 8 h. A piezoelectric objective scanner was used to control the focal plane. At first, the objective was focused on the bottom (0 μm) of the glass-bottom dish. The focal plane continuously moved up to 16 μm in 1 s. At the same time, the camera recorded bright-field images (Video S4) or the SECARS images (Video S5) at a speed of 60 fps. Totally, 60 sections were recorded at a step size of 267 nm. Figure 4a, b shows the bright-field images and the corresponding WISE-CARS images at three axial positions: at the bottom (0 μm), in the middle (8 μm), and at the top (16 μm). At the bottom, the SECARS image shows the nanotags inside cells and the nanotags attached to the glass surface. When the focal plane moves up, the SECARS signals from nanotags outside cells fade away. When the focal plane is at the center of cells, most of the signals originate from the nanotags in the cells. The 3D images of WISE-CARS show the distribution of nanotags at different layers. The 3D projection (Video S6) shows the 3D distributions of nanotags in live cells. Our WISE-CARS microscope only takes 1 s to obtain the 3D images. To estimate the depth resolution of our setup, we select three small particles in the cells and plot their z-profiles, as shown in Figure 4c. The width of z-profiles of nanotags are ca. 2 μm based on Gaussian fitting. This result indicates that WISE-CARS has the capability to visualize the 3D distribution of nanotags in a living cell.

Label-Free Biomolecule Detection. Adenine was selected as a testbed to demonstrate label-free detection of endogenous biomolecules using our WISE-CARS microscope. The pump beam was tuned to 967 nm to cover the desired vibrational region around 724 cm⁻¹. The pump and Stokes laser powers were both 120 mW. First, hyperspectral data cubes from the adenine (N¹⁴A) and adenine-1, 3-¹⁵N₂ (N¹⁵A)-modified Au NPs were recorded at a speed of 60 fps. Figure S1a, b shows the SECARS images of N¹⁴A and N¹⁵A. As shown in Figure S1c, the SERS spectra of N¹⁴A and N¹⁵A showed different Raman bands centered at 741 and 733 cm⁻¹, respectively. Figure S1d shows that such spectral differences could be clearly captured by our WISE-CARS system. Single-pixel SECARS spectra of N¹⁴A and N¹⁵A are shown in Figure

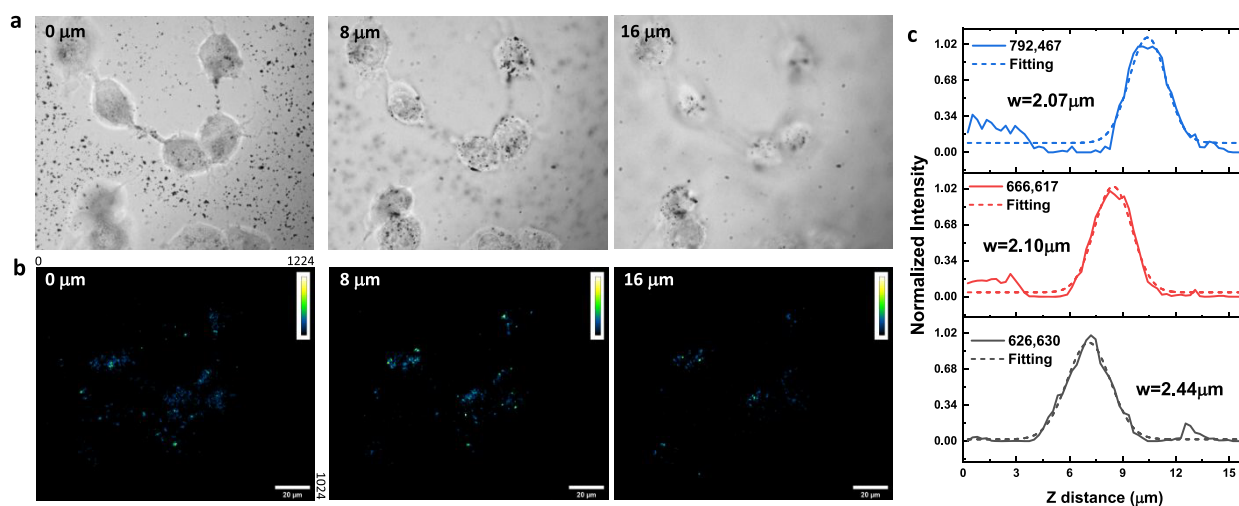


Figure 4. 3D WISE-CARS imaging of nanotags in live cells. (a) Bright-field images of T24 cells at different focal planes. (b) Corresponding SECARS images of T24 cells at 1577 cm⁻¹. (c) Z-profiles of single NP clusters in T24 cells. The scale bar is 20 μm. The inside numbers are the X–Y pixel coordinates where the spectra were recorded.

1e, f. These results collectively indicate that WISE-CARS is capable of imaging biomolecules at a spectral resolution of $\sim 10 \text{ cm}^{-1}$.

We further tested whether WISE-CARS can be used to probe the response of *S. aureus* to starvation stress. *S. aureus* secretes adenine, a purine degradation product when *S. aureus* cells are exposed to a non-nutrient, water-only environment.³⁸ The bacterial suspensions were dropped on the self-assembled Au NP substrate and dried within 10 min. SERS results clearly show that *S. aureus* cells only release adenine byproducts under starvation stress (Figure S2a). Prior to detailed analysis, the SECARS spectra were background-subtracted using the airPLS method to remove the two-color two-photon luminescence background induced by Au NPs.³⁹ The pixel-integrated SECARS spectrum of *S. aureus* after 1 h starvation shows a clear signature peak at 741 cm^{-1} (Figure S2b). In contrast, the SECARS spectrum from the sample without starvation did not display any adenine-like Raman peak. The results match the previous results well.^{38,40}

Because WISE-CARS microscopy can sample millions of pixels on a substrate in 1 s, we further asked whether adenine released from bacteria can be detected at the single-pixel level. Figure 5a shows the spatial distributions of bacteria-secreted adenine on the self-assembled Au NP substrate. As the control group, the SECARS image of normal *S. aureus* cells is shown in Figure 5b. The raw single-pixel spectra from the bright spots in Figure 5a, b are plotted in Figure 5c, d, respectively. The dashed lines in Figure 5c, d are the fitted two-photon luminescence background. After background fitting and removal, the adenine peak at 741 cm^{-1} is clearly seen for the starved bacteria (Figure 5e) but is absent for the normal bacteria (Figure 5f). These “bright spots” we observed in the control sample originate from the photoluminescence of aggregated Au NPs.

DISCUSSION

We developed a WISE-CARS microscope that allows for real-time observing the dynamic spatiotemporal distribution of nanotags in live cells and label-free detection of endogenous biomolecules. Unlike the scanning-based CARS microscope, the acquisition time in the wide-field imaging system is independent of the pixel number. Here, we successfully achieved 120 fps imaging speed (5 times of video rate) with a large field of view (over $130 \mu\text{m}$) and a large pixel number (1224×1024 pixels). In comparison, wide-field SERS needs a sophisticated tunable filter for the acquisition of hyperspectral data. The tunable filter limits the tuning speed and spectral resolutions. Here, with the spectral focusing approach, the spectral tuning of WISE-CARS could be very fast by simply changing the time delay between two laser pulses via a motorized stage. In this way, WISE-CARS can obtain over 1 million spectra within 0.5 s with a 10 cm^{-1} spectral resolution.

Harnessing the plasmonic enhancement, the WISE-CARS microscope requires ultralow power density to excite the CARS process. The estimated average laser power density in WISE-CARS is $0.015 \text{ mW}/\mu\text{m}^2$, which is 30 times lower than previous laser-scanning SECARS and four orders lower than laser-scanning CARS. Such low illumination density opens a great opportunity to implement wide-field chemical imaging with a standard laser of high repetition rate and low pulse energy. The lower pulse energy helps reduce the photodamage that may occur when illuminating the sample with high-energy pulses in conventional CARS microscopy.²⁷ Recent literature

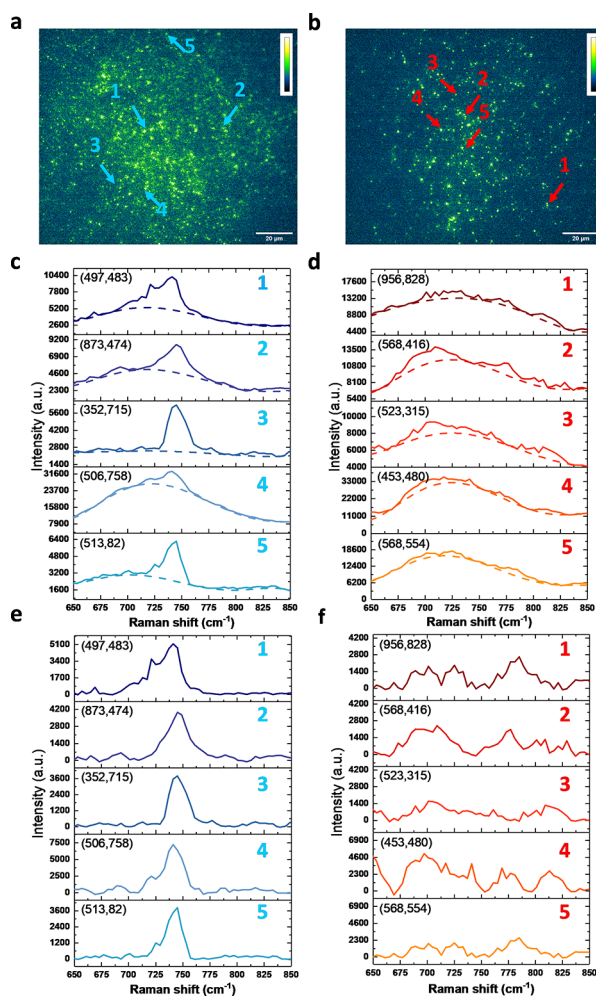


Figure 5. WISE-CARS detection of biomolecules released from starved bacteria. (a) Background-corrected SECARS image of *S. aureus* with 1 h starvation. Raman shift: 741 cm^{-1} . (b) Background-corrected SECARS image of *S. aureus* without starvation. Raman shift: 741 cm^{-1} . (c, d) Raw single-pixel SECARS spectra of *S. aureus* with (1 h, c) and without (0 h, d) starvation. (e, f) Background-corrected single-pixel SECARS spectra of *S. aureus* with (1 h, e) and without (0 h, f) starvation. The labels show the X–Y pixel coordinates where the spectra were recorded. Arrows indicate the locations in the images.

reported wide-field SPP-mediated CARS to image lipid solid samples and dried cells. Although a gold film was used to uniformly amplify signal generation, it also introduced imaging artifacts from the SPP propagations. In addition, SPP only enhanced the signals from the cell membrane region that is in close proximity (100 nm) of the gold film.²⁹ Here, we used the LSPR effect that amplifies the Raman signal inside live cells and enables 3D imaging. Moreover, the enhancement performance of LSPR allows for the amplification with a factor of 10^{10} ,³¹ which is three orders of magnitude stronger than SPP enhancement.³⁰

In addition to SECARS, an alternative method that combined coherent Raman microscopy and the plasmonic effect is plasmon-enhanced stimulated Raman scattering (PESRS) microscopy.^{40,41} However, implementing PESRS in a wide-field geometry is challenging and complicated. Unlike CARS, the SRS signals appear at the same wavelength as the excitation lasers. Thus, optical modulation and lock-in detection are generally used to extract the signals from the

laser pulse in SRS measurement. In principle, to achieve wide-field SRS measurement, one can employ a virtual lock-in camera approach that has been successfully used in wide-field photothermal imaging.⁴² In this approach, pump-on and pump-off images are sequentially recorded using a CMOS camera, and the difference between on and off images produces a chemical image. However, implementing wide-field SRS using this approach is difficult. The main challenge is camera saturation. The maximum pump power saturating a typical CMOS camera sensor can be calculated as $P_{\max} = \frac{E \times N \times S_0}{t \times QE}$. Here, E is the energy per photon (for 888 nm: $E = 2.24 \times 10^{-19}$ J), N is the number of pixels 2448×2048 , S_0 is the full well capacity $45,000 e^-$. t is the camera integration time (1 ms), and QE is the camera quantum efficiency (40%) at the pump wavelength. Based on our calculation, the pump power saturating the camera is about 0.1 mW. Considering that only 1/10 pump power passes through the sample, the maximum power incident on the sample is around 1 mW. Such power on the sample is too low to effectively generate SRS signals. To achieve wide-field SRS, a camera with an ultra-large full well capacity is necessary. Additionally, PESRS displays dispersive line shapes, and its enhancement factor is lower than SECARS,³¹ which complicates data analysis.

The current proof-of-principle study on WISE-CARS may serve as a starting point for further investigations using this plasmon-enhanced nonlinear vibrational imaging technique. Our method can be further developed toward ultrafast 3D imaging of spatiotemporal dynamics of small molecules in live cells. With further substrate development, single-molecule sensitivity^{20,21} is expected to allow for the detection of rare molecules. In addition, by conjugating antibodies or target-specific ligands to plasmonic nanotags labeled with spectrally distinct Raman reporters,¹⁹ high-speed super-multiplex imaging through our hyperspectral WISE-CARS microscope can be envisioned.

■ ASSOCIATED CONTENT

SI Supporting Information

The Supporting Information is available free of charge at <https://pubs.acs.org/doi/10.1021/acsphotonics.1c02015>.

Supporting figure of N¹⁴A and N¹⁵A WISE-CARS detection and supporting figure of the WISE-CARS detection of *S. aureus* adenine secretion under starvation stress (PDF)

Video of the hyperspectral SECARS data cube of Mpy-modified aggregates of Au NPs (MP4)

Video of real-time monitoring nanotags movements inside live T24 cells (MP4)

Video of hyperspectral WISE-CARS imaging of nanotags in live cells (MP4)

Video of 3D bright-field imaging of nanoprobe inside live cells (MP4)

Video of 3D WISE-CARS imaging of nanotags inside live cells (MP4)

Video of 3D projection of nanotags in cells (MP4)

■ AUTHOR INFORMATION

Corresponding Author

Ji-Xin Cheng – Department of Electrical and Computer Engineering, Department of Chemistry, and Department of

Biomedical Engineering, Boston University, Boston, Massachusetts 02215, United States; orcid.org/0000-0002-5607-6683; Email: jxcheng@bu.edu

Authors

Cheng Zong – Department of Electrical and Computer Engineering, Boston University, Boston, Massachusetts 02215, United States

Ran Cheng – Department of Chemistry, Boston University, Boston, Massachusetts 02215, United States

Fukai Chen – Department of Biomedical Engineering, Boston University, Boston, Massachusetts 02215, United States

Peng Lin – Department of Electrical and Computer Engineering, Boston University, Boston, Massachusetts 02215, United States

Meng Zhang – Department of Electrical and Computer Engineering, Boston University, Boston, Massachusetts 02215, United States

Zhicong Chen – Department of Electrical and Computer Engineering, Boston University, Boston, Massachusetts 02215, United States

Chuan Li – Department of Electrical and Computer Engineering, Boston University, Boston, Massachusetts 02215, United States

Chen Yang – Department of Electrical and Computer Engineering and Department of Chemistry, Boston University, Boston, Massachusetts 02215, United States; orcid.org/0000-0001-9454-847X

Complete contact information is available at:

<https://pubs.acs.org/10.1021/acsphotonics.1c02015>

Author Contributions

C.Z. and R.C. contributed equally. Experiments were designed by C.Z. and J.-X.C. C.Z. and R.C. developed the WISE-CARS microscope with the help of P.L. and C.L. The WISE-CARS imaging experiments were conducted by C.Z. and R.C. R.C. and C.Z. synthesized nanoparticles and substrates. Data analysis was executed by C.Z. and R.C. F.C. and Z.C. prepared live-cell samples. M.Z. and R.C. prepared bacteria samples. C.Z. and R.C. wrote the paper, and it was revised by J.-X.C. and C.Y. All authors commented on the manuscript.

Funding

This work was supported by NIH R35 GM136223, R01 AI141439, and NSF CHE1807106 to J.-X.C.

Notes

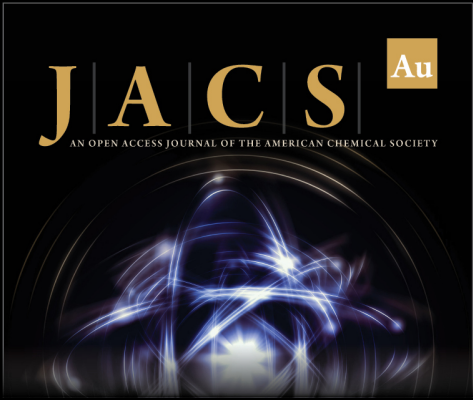
The authors declare no competing financial interest.

■ REFERENCES


- (1) Zong, C.; Xu, M.; Xu, L.-J.; Wei, T.; Ma, X.; Zheng, X.-S.; Hu, R.; Ren, B. Surface-enhanced Raman spectroscopy for bioanalysis: reliability and challenges. *Chem. Rev.* **2018**, *118*, 4946–4980.
- (2) Langer, J.; Jimenez de Aberasturi, D.; Aizpurua, J.; Alvarez-Puebla, R. A.; Auguie, B.; Baumberg, J. J.; Bazan, G. C.; Bell, S. E. J.; Boisen, A.; Brolo, A. G.; Choo, J.; Cialla-May, D.; Deckert, V.; Fabris, L.; Faulds, K.; Garcia de Abajo, F. J.; Goodacre, R.; Graham, D.; Haes, A. J.; Haynes, C. L.; Huck, C.; Itoh, T.; Käll, M.; Kneipp, J.; Kotov, N. A.; Kuang, H.; Le Ru, E. C.; Lee, H. K.; Li, J.-F.; Ling, X. Y.; Maier, S. A.; Mayerhöfer, T.; Moskovits, M.; Murakoshi, K.; Nam, J.-M.; Nie, S.; Ozaki, Y.; Pastoriza-Santos, I.; Perez-Juste, J.; Popp, J.; Pucci, A.; Reich, S.; Ren, B.; Schatz, G. C.; Shegai, T.; Schlücker, S.; Tay, L.-L.; Thomas, K. G.; Tian, Z.-Q.; Van Duyne, R. P.; Vo-Dinh, T.; Wang, Y.; Willets, K. A.; Xu, C.; Xu, H.; Xu, Y.; Yamamoto, Y. S.; Zhao, B.; Liz-Marzán, L. M. Present and Future of Surface-Enhanced Raman Scattering. *ACS Nano* **2020**, *14*, 28–117.

- (3) Willets, K. A.; Van Duyne, R. P. Localized surface plasmon resonance spectroscopy and sensing. *Annu. Rev. Phys. Chem.* **2007**, *58*, 267–297.
- (4) Ding, S.-Y.; Yi, J.; Li, J.-F.; Ren, B.; Wu, D.-Y.; Panneerselvam, R.; Tian, Z.-Q. Nanostructure-based plasmon-enhanced Raman spectroscopy for surface analysis of materials. *Nat. Rev. Mater.* **2016**, *1*, 16021.
- (5) Lindquist, N. C.; Brolo, A. G. Ultra-High-Speed Dynamics in Surface-Enhanced Raman Scattering. *J. Phys. Chem. C* **2021**, *125*, 7523–7532.
- (6) Chen, Y.; Ren, J.-Q.; Zhang, X.-G.; Wu, D.-Y.; Shen, A.-G.; Hu, J.-M. Alkyne-Modulated Surface-Enhanced Raman Scattering-Palette for Optical Interference-Free and Multiplex Cellular Imaging. *Anal. Chem.* **2016**, *88*, 6115–6119.
- (7) Wang, M.; Zhang, C.; Yan, S.; Chen, T.; Fang, H.; Yuan, X. Wide-Field Super-Resolved Raman Imaging of Carbon Materials. *ACS Photonics* **2021**, *8*, 1801–1809.
- (8) Havener, R. W.; Ju, S.-Y.; Brown, L.; Wang, Z.; Wojcik, M.; Ruiz-Vargas, C. S.; Park, J. High-Throughput Graphene Imaging on Arbitrary Substrates with Widefield Raman Spectroscopy. *ACS Nano* **2012**, *6*, 373–380.
- (9) Wang, L.; Dai, Y.; He, H.; Lv, R.; Zong, C.; Ren, B. Dynamic Raman imaging system with high spatial and temporal resolution. *Rev. Sci. Instrum.* **2017**, *88*, No. 095110.
- (10) Kim, J.; Nam, S. H.; Lim, D.-K.; Suh, Y. D. SERS-based particle tracking and molecular imaging in live cells: toward the monitoring of intracellular dynamics. *Nanoscale* **2019**, *11*, 21724–21727.
- (11) Zhang, C.; Zhang, D.; Cheng, J.-X. Coherent Raman scattering microscopy in biology and medicine. *Annu. Rev. Biomed. Eng.* **2015**, *17*, 415–445.
- (12) Liao, C.-S.; Cheng, J.-X. In situ and in vivo molecular analysis by coherent Raman scattering microscopy. *Annu. Rev. Anal. Chem.* **2016**, *9*, 69–93.
- (13) Evans, C. L.; Xie, X. S. Coherent anti-Stokes Raman scattering microscopy: chemical imaging for biology and medicine. *Annu. Rev. Anal. Chem.* **2008**, *1*, 883–909.
- (14) Camp, C. H., Jr.; Cicerone, M. T. Chemically sensitive bioimaging with coherent Raman scattering. *Nat. Photonics* **2015**, *9*, 295–305.
- (15) Evans, C. L.; Potma, E. O.; Puoris'haag, M.; Cote, D.; Lin, C. P.; Xie, X. S. Chemical imaging of tissue in vivo with video-rate coherent anti-Stokes Raman scattering microscopy. *PNAS* **2005**, *102*, 16807–16812.
- (16) Liang, E. J.; Weippert, A.; Funk, J. M.; Materny, A.; Kiefer, W. Experimental observation of surface-enhanced coherent anti-Stokes Raman scattering. *Chem. Phys. Lett.* **1994**, *227*, 115–120.
- (17) Steuwe, C.; Kaminski, C. F.; Baumberg, J. J.; Mahajan, S. Surface enhanced coherent anti-Stokes Raman scattering on nanostructured gold surfaces. *Nano Lett.* **2011**, *11*, 5339–5343.
- (18) Voronine, D. V.; Sinyukov, A. M.; Hua, X.; Wang, K.; Jha, P. K.; Munusamy, E.; Wheeler, S. E.; Welch, G.; Sokolov, A. V.; Scully, M. O. Time-resolved surface-enhanced coherent sensing of nanoscale molecular complexes. *Sci. Rep.* **2012**, *2*, 891.
- (19) Schlücker, S.; Salehi, M.; Bergner, G.; Schütz, M.; Ströbel, P.; Marx, A.; Petersen, I.; Dietzek, B.; Popp, J. Immuno-surface-enhanced coherent anti-Stokes Raman scattering microscopy: immunohistochemistry with target-specific metallic nanoprobe and nonlinear Raman microscopy. *Anal. Chem.* **2011**, *83*, 7081–7085.
- (20) Yampolsky, S.; Fishman, D. A.; Dey, S.; Hulkko, E.; Banik, M.; Potma, E. O.; Apkarian, V. A. Seeing a single molecule vibrate through time-resolved coherent anti-Stokes Raman scattering. *Nat. Photonics* **2014**, *8*, 650–656.
- (21) Zhang, Y.; Zhen, Y.-R.; Neumann, O.; Day, J. K.; Nordlander, P.; Halas, N. J. Coherent anti-Stokes Raman scattering with single-molecule sensitivity using a plasmonic Fano resonance. *Nat. Commun.* **2014**, *5*, 4424.
- (22) Koo, T.-W.; Chan, S.; Berlin, A. A. Single-molecule detection of biomolecules by surface-enhanced coherent anti-Stokes Raman scattering. *Opt. Lett.* **2005**, *30*, 1024–1026.
- (23) Heinrich, C.; Bernet, S.; Ritsch-Martel, M. Wide-field coherent anti-Stokes Raman scattering microscopy. *Appl. Phys. Lett.* **2004**, *84*, 816–818.
- (24) Lei, M.; Winterhalder, M.; Selm, R.; Zumbusch, A. Video-rate wide-field coherent anti-Stokes Raman scattering microscopy with collinear nonphase-matching illumination. *J. Biomed. Opt.* **2011**, *16*, No. 021102.
- (25) Toytman, I.; Cohn, K.; Smith, T.; Simanovskii, D.; Palanker, D. Wide-field coherent anti-Stokes Raman scattering microscopy with non-phase-matching illumination. *Opt. Lett.* **2007**, *32*, 1941–1943.
- (26) Toytman, I.; Simanovskii, D.; Palanker, D. On illumination schemes for wide-field CARS microscopy. *Opt. Express* **2009**, *17*, 7339–7347.
- (27) Silve, A.; Dorval, N.; Schmid, T.; Mir, L. M.; Attal-Tretout, B. A wide-field arrangement for single-shot CARS imaging of living cells. *J. Raman Spectrosc.* **2012**, *43*, 644–650.
- (28) Shen, Y.; Wang, J.; Wang, K.; Sokolov, A. V.; Scully, M. O. Wide-field coherent anti-stokes raman scattering microscopy based on picosecond supercontinuum source. *APL Photonics* **2018**, *3*, 116104.
- (29) Fast, A.; Kenison, J. P.; Syme, C. D.; Potma, E. O. Surface-enhanced coherent anti-Stokes Raman imaging of lipids. *Appl. Opt.* **2016**, *55*, 5994–6000.
- (30) Kenison, J. P.; Fast, A.; Guo, F.; LeBon, A.; Jiang, W.; Potma, E. O. Imaging properties of surface-enhanced coherent anti-Stokes Raman scattering microscopy on thin gold films. *JOSA B* **2017**, *34*, 2104–2114.
- (31) Zong, C.; Xie, Y.; Zhang, M.; Huang, Y.; Yang, C.; Cheng, J.-X. Plasmon-enhanced coherent anti-stokes Raman scattering vs plasmon-enhanced stimulated Raman scattering: Comparison of line shape and enhancement factor. *J. Chem. Phys.* **2021**, *154*, No. 034201.
- (32) Lin, H.; Lee, H. J.; Tague, N.; Lugagne, J.-B.; Zong, C.; Deng, F.; Shin, J.; Tian, H.; Wong, W.; Dunlop, M. J.; Cheng, J. X. Microsecond fingerprint stimulated Raman spectroscopic imaging by ultrafast tuning and spatial-spectral learning. *Nat. Commun.* **2021**, *12*, 3052.
- (33) Kimling, J.; Maier, M.; Okenve, B.; Kotaidis, V.; Ballot, H.; Plech, A. Turkevich method for gold nanoparticle synthesis revisited. *J. Phys. Chem. B* **2006**, *110*, 15700–15707.
- (34) Zheng, X.-S.; Hu, P.; Cui, Y.; Zong, C.; Feng, J.-M.; Wang, X.; Ren, B. BSA-coated nanoparticles for improved SERS-based intracellular pH sensing. *Anal. Chem.* **2014**, *86*, 12250–12257.
- (35) Zheng, X.-S.; Hu, P.; Zhong, J.-H.; Zong, C.; Wang, X.; Liu, B.-J.; Ren, B. Laser power dependent surface-enhanced Raman spectroscopic study of 4-mercaptopyridine on uniform gold nanoparticle-assembled substrates. *J. Phys. Chem. C* **2014**, *118*, 3750–3757.
- (36) Maggioni, M.; Boracchi, G.; Foi, A.; Egiazarian, K. Video denoising, deblocking, and enhancement through separable 4-D nonlocal spatiotemporal transforms. *IEEE Trans. Image Process.* **2012**, *21*, 3952–3966.
- (37) Behzadi, S.; Serpooshan, V.; Tao, W.; Hamaly, M. A.; Alkawareek, M. Y.; Dreaden, E. C.; Brown, D.; Alkilany, A. M.; Farokhzad, O. C.; Mahmoudi, M. Cellular uptake of nanoparticles: journey inside the cell. *Chem. Soc. Rev.* **2017**, *46*, 4218–4244.
- (38) Premasiri, W. R.; Lee, J. C.; Sauer-Budge, A.; Théberge, R.; Costello, C. E.; Ziegler, L. D. The biochemical origins of the surface-enhanced Raman spectra of bacteria: a metabolomics profiling by SERS. *Anal. Bioanal. Chem.* **2016**, *408*, 4631–4647.
- (39) Zhang, Z.-M.; Chen, S.; Liang, Y.-Z. Baseline correction using adaptive iteratively reweighted penalized least squares. *Analyst* **2010**, *135*, 1138–1146.
- (40) Zong, C.; Xie, Y.; Zhang, M.; Huang, Y.; Yang, C.; Cheng, J. X. Plasmon-enhanced stimulated Raman scattering microscopy with single-molecule detection sensitivity. *Nat. Commun.* **2021**, *154*, No. 034201.
- (41) Frontiera, R. R.; Henry, A.-I.; Gruenke, N. L.; Van Duyne, R. P. Surface-enhanced femtosecond stimulated Raman spectroscopy. *J. Phys. Chem. Lett.* **2011**, *2*, 1199–1203.


(42) Bai, Y.; Zhang, D.; Lan, L.; Huang, Y.; Maize, K.; Shakouri, A.; Cheng, J.-X. Ultrafast chemical imaging by widefield photothermal sensing of infrared absorption. *Sci. Adv.* **2019**, *5*, No. eaav7127.




JACS Au
AN OPEN ACCESS JOURNAL OF THE AMERICAN CHEMICAL SOCIETY



Editor-in-Chief
Prof. Christopher W. Jones
Georgia Institute of Technology, USA

Open for Submissions 

pubs.acs.org/jacsau  ACS Publications
Most Trusted. Most Cited. Most Read.